Power-Tolerant NOMA Using Data-Aware Adaptive Power Assignment for IoT Systems

Hamad Yahya, *Graduate Student Member, IEEE*, Arafat Al-Dweik, *Senior Member, IEEE*, and Emad Alsusa, *Senior Member, IEEE*

***Abstract*—Nonorthogonal multiple access (NOMA) is a promising candidate for future wireless networks due to its ability to improve the spectral efficiency and network connectivity. Nevertheless, the error rate performance of NOMA depends significantly on the power assignment for each user, which requires accurate knowledge of the channel state information (CSI) at the transmitter, which can be challenging for several applications, such as wireless sensor networks (WSNs) and Internet of Things (IoT). Therefore, this article proposes a power-tolerant NOMA by adaptively changing the signal power of each user to reduce the system sensitivity to inaccurate power assignment. The power adaptation in the power-adaptive NOMA (PANOMA) is performed based on the transmitted data, and it does not require accurate CSI. To quantify its potential, the bit error rate (BER) and the lower bound capacity performance, over Rayleigh fading channels, are derived in exact closed forms for two and three users scenarios. The results demonstrate that PANOMA provides a tangible BER performance improvement over conventional power-domain NOMA when both schemes use suboptimal power assignment, which is typically experienced in practical scenarios involving channel time variation and CSI estimation errors. Specifically, it will be shown that both schemes provide similar BERs using optimal assignment, but the PANOMA offers BER reduction by a factor of 10 for certain scenarios when suboptimal power values are assigned. The integrity of the analytical results is verified via matching extensive Monte Carlo simulation experiments.**

***Index Terms*—Interference alignment, interference management, nonorthogonal multiple access (NOMA), power assignment, sum rate.**

I. Introduction

IT IS widely acknowledged that the number of devices connected to mobile networks will continue to grow at a tremendous pace. According to [1], by the end of 2020, the number of devices will reach 25 billion, which is far beyond the number of devices connected to wireless networks a few years back. The reason for this substantial increase is the unfolding evolution of traditional cities and homes toward becoming smart. This includes applications under the umbrella of the Internet-of-Things (IoT) and machine-to-machine (M2M) communications, which play a central role in many applications, such as waste management, smart transportation systems, and smart buildings [2]–[5]. To support these applications, the fifth generation (5G) of wireless networks is designed to provide an agile data transport infrastructure with capabilities that include massive connectivity, larger spectral efficiency, and low latency [6]. For instance, according to the 5G standard, narrowband IoT (NB-IoT) will support the massive connectivity of low-cost-low-capability devices [7], which are known to have low data-rate requirements akin to wireless sensor networks (WSNs) [8]. The responsibility to satisfy such requirements lies mostly within the multiple access functionality of the communication system [9]. In current and previous mobile communication systems, orthogonal multiple access (OMA) techniques are mostly used, which include frequency-division multiple access (FDMA), time-division multiple access (TDMA), and orthogonal FDMA (OFDMA). Moreover, code-division multiple access (CDMA) can also be considered an OMA technique when orthogonal spreading sequences are used. In general, most wireless standards, including 5G, can be considered OMA based, where the resources are allocated to the users of one cell in such a way to prevent mutual interference.

Meanwhile, recent advances in nonorthogonal multiple access (NOMA), particularly interference cancellation (IC) to separate the users' signals at the receiver. IC techniques include parallel IC (PIC) and successive IC (SIC), with the usual benchmark being the optimum maximum-likelihood detector (MLD) [5]. It is shown in [5] that SIC outperforms PIC when each user is allocated a unique power value. Furthermore, PIC can be computationally inefficient as it requires a large number of iterations to provide an acceptable bit error rate (BER) [10]. In [11], it is claimed that SIC can overcome propagation errors using an iterative approach.

As a key performance metric, the BER of NOMA has been considered by several researchers [12]–[18]. In [14], an exact closed-form solution is derived for the downlink BER of two-user NOMA in a single-input–single-output (SISO) Rayleigh fading broadcast channel with imperfect SIC. The exact BER for two- and three-user downlink NOMA is derived in [15] for Nakagami-*m* fading channels using quadrature phase-shift keying (QPSK). In [18], the BER for downlink NOMA with an arbitrary number of users is derived for the Rayleigh

Manuscript received August 30, 2020; revised December 21, 2020 and January 28, 2021; accepted April 9, 2021. Date of publication April 13, 2021; date of current version September 23, 2021. The work of Arafat Al-Dweik was supported by Khalifa University Competitive Internal Research Awards under Grant CIRA-2020-056. *(Corresponding author: Arafat Al-Dweik.)*

Hamad Yahya and Emad Alsusa are with the Department of Electrical and Electronic Engineering, The University of Manchester, Manchester M13 9PL, U.K. (e-mail: hamad.mohamadaliyahya@manchester.ac.uk; e.alsusa@manchester.ac.uk).

Arafat Al-Dweik is with the Center for Cyber Physical Systems, Khalifa University, Abu Dhabi, UAE, and also with the Department of Electrical and Computer Engineering, Western University, London, ON N6A 3K7, Canada (e-mail: dweik@fulbrightmail.org; arafat.dweik@ku.ac.ae).

Digital Object Identifier 10.1109/JIOT.2021.3072985

fading channel where all users adopt binary phase-shift keying (BPSK). The analysis is extended for the quadrature amplitude modulation (QAM) in [19]. The BER results presented in [12]–[19] show that the BER of NOMA systems degrades by IUI, which can be significant if the users' power allocation is not performed diligently.

Power assignment in NOMA can be generally designed to be fixed or dynamic. Fixed power assignment has low complexity and does not require prior knowledge of the channel state information (CSI) at the transmitter [12], [13], [16], [18], [20]. However, it cannot satisfy the users' BER requirements or minimize the average BER. Alternatively, dynamic power assignment has the potential to satisfy Quality-of-Service (QoS) requirements and minimize the BER. Dynamic power assignment typically uses the instantaneous or statistical CSI to allocate the power for each user [14], [15], [17], [21]. The assigned power can be considered optimum if it is used to minimize certain performance metrics such as the BER. Because the power assignment is performed at the transmitter side, accurate CSI should be priorly available at the transmitter, which is highly challenging for mobile channels and requires substantial feedback overhead. Adaptive power assignment with in accurate or outdated CSI will not be optimal and may cause severe BER degradation. In the literature, very little work has considered reducing the BER sensitivity to nonoptimal power assignment. For example, interference alignment is proposed in [21] to improve the symbol error rate (SER) and support high-reliability low-latency IoT systems. Dynamic power allocation is applied using statistical CSI to minimize the average asymptotic SER. Although the system offers SER improvement and resilience to nonoptimal power assignment, the system requires significant computational complexity, the detection process requires pilot symbols to avoid detection ambiguity, and the system is limited only to a two-user NOMA. Robust NOMA design with respect to sum rate and energy efficiency is considered in [22]–[24]. However, such schemes are not generally applicable to the BER scenario, and they require substantial computational power.

Other approaches for improving the BER of NOMA include applying a particular phase rotation for each user while keeping the power for each user fixed, as well as incorporating signal space diversity through inphase/quadrature interleaving [25]. The presented results show that a gain of about 1.3 dB can be obtained, but only for one of the users. Furthermore, the achieved gain depends on the time/frequency selectivity of the channel, and becomes less significant in flat fading channels. It is worth noting that this approach increases the transmitter and receiver complexity due to the additional operations required to modulate and recover the data symbols. Qiu *et al.* [26] proposed a class of NOMA schemes where all users' signals are mapped into n-dimensional constellations that correspond to the same algebraic lattices to enable every user achieve full diversity. The presented results show a significant BER improvement at the expense of substantial additional complexity. Such design is based on the assumption that each symbol experiences independent and identically distributed (i.i.d.) channels, which is a limiting assumption as the channel coefficients are highly correlated in slow-fading channels, unless interleavers with very depth are used.

A. Motivation and Contribution

As can be noted from the aforementioned discussions, the BER of NOMA is highly sensitive to the users' power assignment, particularly for IoT systems, where accurate CSI is typically difficult to obtain [8]. Moreover, most IoT applications are based on short-length packets and, thus, frequent CSI feedback may degrade the system efficiency significantly. For example, in fourth generation (4G) and 5G networks, the CSI feedback typically requires 22 bits [27]. Consequently, link adaptation in IoT applications should be designed to be robust to inaccurate CSI conditions. Therefore, this article proposes a power-tolerant data-aware adaptive power assignment technique to improve the BER performance of power-domain NOMA in scenarios where optimal power allocation cannot be maintained. The overall idea is motivated by the fact that prior knowledge of IUI is available at the transmitter, hence it can be utilized to adapt the power per NOMA symbol depending on whether IUI is constructive or destructive. It is shown that the proposed data-aware power-adaptive NOMA (PANOMA) scheme maintains the signal-to-noise ratio at the receivers almost unchanged and, hence, the BER and capacity experience negligible degradation as compared to NOMA.

The contributions of this article can be summarized as follows.

1) We propose a data-aware power assignment for power-domain NOMA IoT systems to improve the system robustness to imperfect power assignments.
2) We derive closed-form BER expressions for the NOMA and PANOMA for two and three users cases using BPSK.
3) We evaluate the impact of nonoptimal power assignment on the NOMA and PANOMA systems.
4) We extend the proposed system to QPSK modulation and determine the BER performance gain. Interestingly, it is shown that the inphase and quadrature components for each user should be assigned different power to minimize the BER.
5) We evaluate the overall lower bound capacity of both systems and quantifying the PANOMA gain for BPSK and QPSK.

B. Article Organization

The remainder of this article is organized as follows. In Section II, the system and the channel models are introduced. In Section III, conditional BER expressions are derived for two users NOMA and PANOMA, while Section IV handles the three users case. Section V derives the unconditional BER, while Section VI presents the basic formulas used to find the lower bound capacity. Section VII presents the analytical and Monte Carlo simulation results. Finally, Section VIII concludes this article with a summary of the main findings and future work.

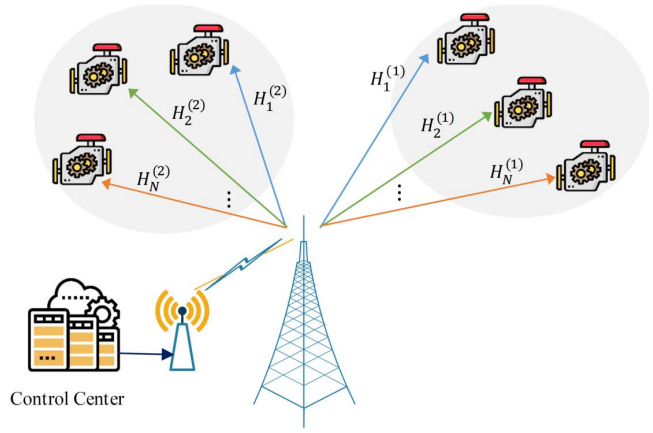

Fig. 1. Illustrative diagram of a NOMA-IoT system where users are clustered in groups of three users and served by one NOMA signal.

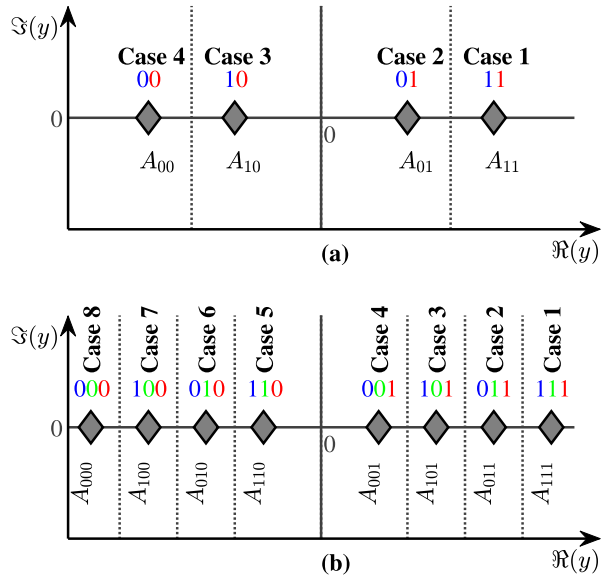

Fig. 2. Constellation diagram of the transmitted signal when BPSK is used by all users. (a) $N = 2$. (b) $N = 3$.

II. System and Channel Models

A. Conventional Power-Domain NOMA

As depicted in Fig. 1, this work considers the downlink of an IoT network where a control center communicates with a large number of IoT devices, also denoted as users, which are mostly actuators. To increase the system spectral efficiency, NOMA is deployed at the base station where each group of N IoT devices is configured to share the same transmission resources simultaneously. Therefore, the base station multiplexes the information symbols of N devices by assigning each user a distinct power coefficient based on the channel conditions. Without loss of generality, we assume that the N users are ordered in ascending order of their channel envelope, i.e., $|H_1| > |H_2| > \cdots > |H_N|$, where H_n, $1 \leq n \leq N$, is the complex channel gain of the link between the base station and the nth user, which is denoted as U_n. Therefore, the power allocation is performed such that a user with severe fading conditions is assigned higher power than a user with good channel conditions [14], [15]. In such scenarios, the power coefficients $\{\alpha_1, \alpha_2, \ldots, \alpha_N\}$ are assigned such that $\alpha_1 < \alpha_2 < \cdots < \alpha_N$, where $\sum_{n=1}^{N} \alpha_n = 1$. The SC process at the base station is described by

$$x_{SC} = \sum_{n=1}^{N} \sqrt{\alpha_n} x_n \tag{1}$$

where x_n is the information symbol of the nth user drawn uniformly from an M-ary phase-shift keying (MPSK) or QAM constellation χ_n. The average power of the transmitted NOMA symbols is normalized to unity such that $E[|x_{SC}|^2] = 1$, where x_{SC} is the transmitted NOMA symbol, and $E[\cdot]$ denotes the expected value. Fig. 2 shows the constellation diagram of the resultant superposition NOMA symbol for $N = 2$ and 3 using BPSK modulation. For $N = 2$, the NOMA constellation consists of four constellation points, with four different amplitudes. Moreover, it can be noted that the leftmost bit belongs to U_1, while the rightmost bit belongs to U_2. The same argument applies for cases where $N > 2$, and when the modulation orders are more than 2.

At the receiver front end, the received baseband signal in flat fading channels is written as

$$y_n = H_n x_{SC} + W_n \tag{2}$$

where $W_n \sim \mathcal{CN}(0, \sigma^2_{W_n})$ is the additive white Gaussian noise (AWGN). In channels with small-scale Rayleigh fading and large-scale path loss, the channel gain $H_n = \sqrt{\beta_n} \times h_n$, $h_n \sim \mathcal{CN}(0, \sigma^2_{h_n})$, $\beta_n = d_n^{-\lambda}$, d_n is the distance between the base station and U_n, and λ is the path-loss exponent. The small-scale fading of different users is considered i.i.d. [25], [26]. Given that CSI is known perfectly at the receiver, the information symbols can be recovered using the joint-multiuser MLD (JMLD)

$$\{\widehat{x}_1, \widehat{x}_2, \ldots, \widehat{x}_N\} = \arg \min_{x_i \in \chi_i} \left| y_n - H_n \sum_{i=1}^{N} \sqrt{\alpha_i} x_i \right|^2 \tag{3}$$

where $\{\widehat{x}_1, \widehat{x}_2, \ldots, \widehat{x}_N\}$ are the jointly detected N users' symbols. Alternatively, the SIC detector can be applied where the symbols of the user with maximum power U_N is detected first using a single-user (SU) MLD while considering all other users' signals as unknown noise. For the user with the second highest power, U_{N-1}, it has to detect and subtract the symbols of U_N, and then apply an SU MLD to detect its own symbols. The minimum power user U_1 has to detect and subtract the symbols of $N-1$ users before it can detect its own symbols. It is worth noting that the SIC and JMLD detectors have identical BER performance, but the SIC has lower complexity [28].

The power assignment for each user may have a significant effect on the performance of all users, and inappropriate power assignment can therefore result in noticeable performance degradation. Therefore, extensive research has been focused on optimal power assignment as reported in [14], [15], [17], and the references listed therein. For the BER case, the power optimization problem is nonlinear hence it is typically solved using certain searching methods, which achieve near-optimal solutions. Moreover, optimal power assignment requires perfect knowledge of the channel statistical information [14], [15],

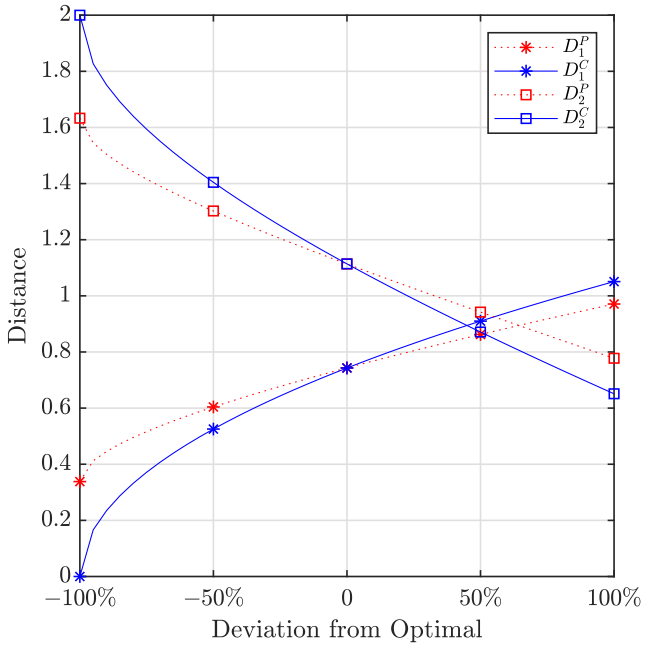

Fig. 3. Euclidean distance versus deviation from optimal power at $E_b/N_0 = 35$ dB.

which is typically very challenging to obtain, particularly in time-varying channels.

B. PANOMA Scheme

To simplify the presentation of the proposed PANOMA scheme, we consider the two users scenario using BPSK modulation. As can be noted from (1) and Fig. 2(a), the constellation points of the two rightmost NOMA symbols are $A_{11} = (\sqrt{\alpha_1} + \sqrt{\alpha_2})$ and $A_{01} = (-\sqrt{\alpha_1} + \sqrt{\alpha_2})$. Therefore, the error event with respect to U_1 is largely determined by the Euclidean distance $D_1^C = |A_{11} - A_{01}| = 2\sqrt{\alpha_1}$. Given that the value of α_1 is selected to minimize the BER, the value of D_1^C will be maximized. However, a small deviation in α_1 from the optimal value will reduce D_1^C from its maximum value and cause BER degradation.

Inspired by the interference alignment principle [29], [30], the power assignment is performed adaptively based on the values of the transmitted symbols of both users. Therefore, the power is assigned based on the user index and values of the information symbols of the two users. Consequently, the transmitted PANOMA symbol is written in a conditional form to capture the dependency of the power on the information symbols. Therefore

$$x_{SC} = \sum_{n=1}^{N} \sqrt{(\alpha_n | [x_1, x_2, \ldots, x_N])} x_n. \tag{4}$$

To reduce the sensitivity of the BER to power assignment process, the power for certain symbols is fixed regardless of the channel conditions, while the power for the remaining symbols can be selected to minimize the average BER. For example, given that $N = 2$ and BPSK is used for both users, the power assignment for the identical symbols cases can be performed such that $\alpha_1|[1, 1] = \alpha_1|[-1, -1] = 0.5$ which is always fixed. However, the power assignment for the symbols with opposite polarities, $\alpha_1|[1, -1]$ and $\alpha_1|[-1, 1]$, can be selected to minimize the average BER using the formula derived in Section III. Therefore, the transmitted NOMA symbol can be expressed as

$$x_{SC} = \begin{cases} \sqrt{\frac{1}{2}}x_1 + \sqrt{\frac{1}{2}}x_2, & x_1 = x_2 \\ \sqrt{\alpha_1}x_1 + \sqrt{\alpha_2}x_2, & x_1 = -x_2. \end{cases} \tag{5}$$

It is worth noting that the equal power selection $\alpha_1 = \alpha_2 = 1/2$ for the case of $x_1 = x_2$ maximizes the NOMA symbol power for the identical symbols case, which can be verified by computing

$$\frac{\partial}{\partial \alpha_1} x_{sc}^2 | [x_1 = x_2] = \frac{1 - 2\alpha_1}{\sqrt{\alpha_1(1 - \alpha_1)}} \tag{6}$$

which is maximum when $\alpha_1 = 1/2$. Similar to the conventional NOMA case, the average power of the PANOMA symbols should be normalized to unity. By comparing the Euclidean distance of the rightmost PANOMA symbols $D_1^P = |A_{11} - A_{01}| = \sqrt{2} + \sqrt{\alpha_1} - \sqrt{\alpha_2}$ to $D_1^C = 2\sqrt{\alpha_1}$, it can be noted that the constant scalar in D_1^P limits its variation with α_1.

The optimal power assignment of U_1 and U_2 for various E_b/N_0 is shown in Table I given that $\beta_1 = 0$ dB and $\beta_2 = 6$ dB where SNR $\triangleq 1/\sigma_W^2$. Fig. 3 shows the distance D_1 and D_2 for NOMA and PANOMA versus the deviation from the optimal power, where $D_2 = |A_{01} - A_{10}|$. As can be noted from the figure, D_1 and D_2 for PANOMA change at a lower rate than NOMA, implying that they remain close to the optimum values. The same conclusion can be made by noting the optimal power values in Table I, where the values of α_1 for Cases 2 and 3 remain roughly unchanged when E_b/N_0 is changed from 15 to 35 dB. Following the same approach for $N = 2$, PANOMA can be applied to $N = 3$. The optimal power coefficients for all users at various E_b/N_0 are shown in Table II where $\beta_1 = 0$ dB, $\beta_2 = 6$ dB, and $\beta_3 = 12$ dB, and Fig. 2(b) shows the constellation diagram.

The PANOMA principle can be extended to higher modulation orders such as QPSK where the inphase and quadrature components are assigned different power factors by treating each dimension independently. Therefore

$$x_{SC} = \sum_{n=1}^{N} \sqrt{\alpha_n^{\Re} | \Re[x_1, x_2, \ldots, x_N]} \Re(x_n) + j\sqrt{\alpha_n^{\Im} | \Im[x_1, x_2, \ldots, x_N]} \Im(x_n) \tag{7}$$

TABLE I
OPTIMAL POWER ASSIGNMENT FOR PANOMA USING VARIOUS E_b/N_0, $N = 2$

Case	Bits	Amplitude	α_1		
			15 dB	25 dB	35 dB
1	11	A_{11}	0.5	0.5	0.5
2	01	A_{01}	0.118	0.113	0.113
3	10	A_{10}	0.118	0.113	0.113
4	00	A_{00}	0.5	0.5	0.5

TABLE II
OPTIMAL POWER ASSIGNMENT FOR PANOMA USING VARIOUS E_b/N_0, $N = 3$

Case #	Bits	Amplitude	$\alpha_1, \alpha_2, \alpha_3$		
			15 dB	**25 dB**	**35 dB**
1	111	A_{111}	$1/3, 1/3, 1/3$	$1/3, 1/3, 1/3$	$1/3, 1/3, 1/3$
2	011	A_{011}	$0.05, 0.475, 0.475$	$0.05, 0.475, 0.475$	$0.05, 0.475, 0.475$
3	101	A_{101}	$0.074, 0.202, 0.724$	$0.072, 0.206, 0.722$	$0.075, 0.208, 0.717$
4	001	A_{001}	$0.075, 0.075, 0.85$	$0.075, 0.075, 0.85$	$0.075, 0.075, 0.85$
5	110	A_{110}	$0.075, 0.075, 0.85$	$0.075, 0.075, 0.85$	$0.075, 0.075, 0.85$
6	010	A_{010}	$0.074, 0.202, 0.724$	$0.072, 0.206, 0.722$	$0.075, 0.208, 0.717$
7	100	A_{100}	$0.05, 0.475, 0.475$	$0.05, 0.475, 0.475$	$0.05, 0.475, 0.475$
8	000	A_{000}	$1/3, 1/3, 1/3$	$1/3, 1/3, 1/3$	$1/3, 1/3, 1/3$

where $\alpha_n^{\Re}$ and $\alpha_n^{\Im}$ are the power coefficients for the inphase and quadrature components, and $\Re(\cdot)$ and $\Im(\cdot)$ represent the real and imaginary parts, respectively.

As can be noted from (4) and (5), the data symbols of U_2 can be detected similar to conventional NOMA, i.e., using SU MLD while considering all other users' symbols as unknown noise. For U_1, the SIC detector cannot be applied directly because the power assigned to U_1 might be either 0.5 or α_1. Therefore, the JMLD shown in (3) can be applied by considering the SC process in (4), or equivalently, a modified SIC detector can be applied. For example, when BPSK with $N = 2$ is used, as shown in Fig. 2(a), the interference can be canceled by computing $\tilde{y} = y_1 - 0.5H_1(\sqrt{2} + \sqrt{\alpha_2} - \sqrt{\alpha_1})\hat{x}_2$. Then, an SU MLD can be used to extract the data symbols of U_1. The same approach can be applied for the case where $N > 2$ and using higher order modulations. Therefore, the proposed system complexity is identical to conventional NOMA. It is worth noting that the systems proposed in [21] and [25] require pilot sequences to perform the detection process, which affects the spectral efficiency. Moreover, the receiver complexity is higher than conventional NOMA.

III. CONDITIONAL BER ANALYSIS, $N = 2$

The analysis in this article focuses on BPSK for both the NOMA and PANOMA, and it is straightforward to extend it to QPSK. These modulation schemes are adopted in various standards, such as the NB-IoT and WiFi standards [7], [31] to provide reliable communications over severe channels. The analysis is general in the sense that can be applied to NOMA and PANOMA regardless the power assignment, which is unique for each particular system. There are four possible cases for each user as shown in Fig. 2(a) where the constellation points of the SC signal are specified. The BER can be obtained by considering all the possible cases. For equally probable symbols, the conditional BER is

$$P_{B_n|\boldsymbol{\gamma}_n} = \frac{1}{2^N}\sum_{i=1}^{2^N} P_{B_n}^{(i)} \tag{8}$$

where $\boldsymbol{\gamma}_n = [\gamma_{1,n}, \gamma_{2,n}, \ldots, \gamma_{L,n}]$, $\gamma_{l,n}$ is a factor that depends on the SNR and symbol power, and L is the total number of possible values for the nth user.

A. Near User (U_1)

Case 1: The transmitted amplitude in this case is A_{11}. The transmitted symbol is detected erroneously if the AWGN level shifts the transmitted symbol to one of the decision regions where the bit value is flipped. Therefore

$$\begin{aligned} P_{B_1}^{(1)} &= \Pr(w < -\{A_{11} - a_{11} - a_{01}\}) \\ &\quad - \Pr(-\{A_{11} + a_{11} + a_{01}\} < w < -A_{11}) \end{aligned} \tag{9}$$

where $a_{b_1b_2} = A_{b_1b_2}/2$, $w \triangleq \Re(W)$, and the user index is dropped from w for notational simplicity. Thus

$$\begin{aligned} P_{B_1}^{(1)} &= \frac{1}{\sqrt{2\pi\sigma_w^2}}\int_{-\infty}^{-a_{11}+a_{01}} \exp\left(\frac{-w^2}{2\sigma_w^2}\right)dw \\ &\quad - \frac{1}{\sqrt{2\pi\sigma_w^2}}\int_{-3a_{11}-a_{01}}^{-A_{11}} \exp\left(\frac{-w^2}{2\sigma_w^2}\right)dw \\ &= \mathrm{Q}\big(\sqrt{\gamma_{1,1}}\big) + \mathrm{Q}\big(\sqrt{\gamma_{2,1}}\big) - \mathrm{Q}\big(\sqrt{\gamma_{4,1}}\big) \end{aligned} \tag{10}$$

where Q(.) is the Gaussian function, and the definitions of $\gamma_{l,n}$ can be found in Table III in the Appendix.

Case 2: The transmitted amplitude is A_{01} and the error event can be computed as the sum of two events, i.e., $P_{B_1}^{(2)} = P_{B_1}^{(2a)} + P_{B_1}^{(2b)}$, where

$$\begin{aligned} P_{B_1}^{(2a)} &= \Pr(w > \{a_{11} + a_{01} - A_{01}\}) \\ &= \mathrm{Q}\big(\sqrt{\gamma_{1,1}}\big) \end{aligned} \tag{11}$$

and

$$\begin{aligned} P_{B_1}^{(2b)} &= \Pr(w < -A_{01}) - \Pr(w < -\{A_{01}+a_{11}+a_{01}\}) \\ &= \mathrm{Q}\big(\sqrt{\gamma_{3,1}}\big) - \mathrm{Q}\big(\sqrt{\gamma_{5,1}}\big). \end{aligned} \tag{12}$$

Thus

$$P_{B_1}^{(2)} = \mathrm{Q}\big(\sqrt{\gamma_{1,1}}\big) + \mathrm{Q}\big(\sqrt{\gamma_{3,1}}\big) - \mathrm{Q}\big(\sqrt{\gamma_{5,1}}\big). \tag{13}$$

For the remaining cases, Cases 3 and 4, the BER is equal in Cases 2 and 1, respectively. Therefore, the conditional BER of U_1 is given by

$$P_{B_1|\boldsymbol{\gamma}_1} = \sum_{i=1}^{5} c_i \mathrm{Q}\big(\sqrt{\gamma_{i,1}}\big) \tag{14}$$

where $\mathbf{c} = (1/2)[2, 1, 1, -1, -1]$.

B. Far User (U_2)

Case 1: The same transmitted amplitude as in U_1. However, its decision boundary is zero. Therefore, the conditional BER is

$$\begin{aligned} P_{B_2}^{(1)} &= \Pr(w < -A_{11}) \\ &= \mathrm{Q}\big(\sqrt{\gamma_{1,2}}\big). \end{aligned} \tag{15}$$

Case 2: The transmitted amplitude is A_{01}. Thus, the conditional BER is

$$\begin{aligned} P_{B_2}^{(2)} &= \Pr(w < -A_{01}) \\ &= \mathrm{Q}\big(\sqrt{\gamma_{2,2}}\big). \end{aligned} \tag{16}$$

The remaining cases, Cases 3 and 4, have identical BER to their peers, Cases 1 and 2, respectively. From now on, only the positive side will be mentioned in the analysis as the negative side is identical to the positive side. Consequently, the conditional BER is

$$P_{B_2}|\boldsymbol{\gamma}_2 = \sum_{i=1}^{2} c_i \mathrm{Q}\big(\sqrt{\gamma_{i,2}}\big) \tag{17}$$

where $\mathbf{c} = (1/2)[1, 1]$.

IV. Conditional BER Analysis, $N = 3$

Similar to the previous section, however, the number of users is 3. The amplitude of the transmitted symbol is determined by the three power coefficients, α_1, α_2, and α_3. Therefore, there are eight possible cases for each user as shown in Fig. 2(b). The same strategy to get the BER will be followed here as well.

A. Near User (U_1)

Case 1: The transmitted amplitude is A_{111}. The BER of this case is shown in (18). Note that the definitions of $\gamma_{l,n}$ can be found in Table IV in the Appendix

$$\begin{aligned} P_{B_1}^{(1)} &= \Pr\left(w < -\{A_{111} - a_{111} - a_{011}\}\right) \\ &\quad - \Pr(-\{A_{111} - a_{101} - a_{001}\} < w < \\ &\qquad - \{A_{111} - a_{011} - a_{101}\}) \\ &\quad - \Pr\left(-\{A_{111} + a_{101} + a_{001}\} < w < -A_{111}\right) \\ &\quad - \Pr(-\{A_{111} + a_{111} + a_{011}\} < w < \\ &\qquad - \{A_{111} + a_{011} + a_{101}\}) \\ &= \mathrm{Q}\big(\sqrt{\gamma_{1,1}}\big) + \mathrm{Q}\big(\sqrt{\gamma_{2,1}}\big) + \mathrm{Q}\big(\sqrt{\gamma_{3,1}}\big) + \mathrm{Q}\big(\sqrt{\gamma_{4,1}}\big) \\ &\quad - \mathrm{Q}\big(\sqrt{\gamma_{14,1}}\big) - \mathrm{Q}\big(\sqrt{\gamma_{15,1}}\big) - \mathrm{Q}\big(\sqrt{\gamma_{16,1}}\big). \end{aligned} \tag{18}$$

Case 2: The transmitted amplitude is A_{011}. The error can be computed as the sum of two events, i.e., $P_{B_1}^{(2)} = P_{B_1}^{(2a)} + P_{B_1}^{(2b)}$, where

$$\begin{aligned} P_{B_1}^{(2a)} &= \Pr(w > \{a_{111} + a_{011} - A_{011}\}) \\ &= \mathrm{Q}\big(\sqrt{\gamma_{1,1}}\big) \end{aligned} \tag{19}$$

and

$$\begin{aligned} P_{B_1}^{(2b)} &= \Pr(w < -\{A_{011} - a_{011} - a_{101}\}) \\ &\quad - \Pr\left(-A_{011} < w < -\{A_{011} - a_{101} - a_{001}\}\right) \\ &\quad - \Pr(-\{A_{011} + a_{011} + a_{101}\} < w < \\ &\qquad - \{A_{011} + a_{101} + a_{001}\}) \\ &\quad - \Pr\left(w < -\{A_{011} + a_{111} + a_{011}\}\right) \\ &= \mathrm{Q}\big(\sqrt{\gamma_{5,1}}\big) + \mathrm{Q}\big(\sqrt{\gamma_{6,1}}\big) + \mathrm{Q}\big(\sqrt{\gamma_{7,1}}\big) \\ &\quad - \mathrm{Q}\big(\sqrt{\gamma_{17,1}}\big) - \mathrm{Q}\big(\sqrt{\gamma_{18,1}}\big) - \mathrm{Q}\big(\sqrt{\gamma_{19,1}}\big). \end{aligned} \tag{20}$$

Thus

$$\begin{aligned} P_{B_1}^{(2)} &= \mathrm{Q}\big(\sqrt{\gamma_{1,1}}\big) + \mathrm{Q}\big(\sqrt{\gamma_{5,1}}\big) + \mathrm{Q}\big(\sqrt{\gamma_{6,1}}\big) + \mathrm{Q}\big(\sqrt{\gamma_{7,1}}\big) \\ &\quad - \mathrm{Q}\big(\sqrt{\gamma_{17,1}}\big) - \mathrm{Q}\big(\sqrt{\gamma_{18,1}}\big) - \mathrm{Q}\big(\sqrt{\gamma_{19,1}}\big). \end{aligned} \tag{21}$$

Case 3: The transmitted amplitude is A_{101}. Similarly, the error can be computed as the sum of two events, i.e., $P_{B_1}^{(3)} = P_{B_1}^{(3a)} + P_{B_1}^{(3b)}$, where

$$\begin{aligned} P_{B_1}^{(3a)} &= \Pr(w > \{a_{011} + a_{101} - A_{101}\}) \\ &\quad - \Pr(w > \{a_{111} + a_{011} - A_{101}\}) \\ &= \mathrm{Q}\big(\sqrt{\gamma_{5,1}}\big) - \mathrm{Q}\big(\sqrt{\gamma_{20,1}}\big) \end{aligned} \tag{22}$$

and

$$\begin{aligned} P_{B_1}^{(3b)} &= \Pr(w < -\{A_{101} - a_{101} - a_{001}\}) \\ &\quad - \Pr(-\{A_{101} + a_{101} + a_{001}\} < w < -A_{101}) \\ &\quad - \Pr(-\{A_{101} + a_{111} + a_{011}\} < w < \\ &\qquad - \{A_{101} + a_{011} + a_{101}\}) \\ &= \mathrm{Q}\big(\sqrt{\gamma_{8,1}}\big) + \mathrm{Q}\big(\sqrt{\gamma_{9,1}}\big) + \mathrm{Q}\big(\sqrt{\gamma_{10,1}}\big) \\ &\quad - \mathrm{Q}\big(\sqrt{\gamma_{21,1}}\big) - \mathrm{Q}\big(\sqrt{\gamma_{22,1}}\big). \end{aligned} \tag{23}$$

Thus

$$\begin{aligned} P_{B_1}^{(3)} &= \mathrm{Q}\big(\sqrt{\gamma_{5,1}}\big) + \mathrm{Q}\big(\sqrt{\gamma_{8,1}}\big) + \mathrm{Q}\big(\sqrt{\gamma_{9,1}}\big) + \mathrm{Q}\big(\sqrt{\gamma_{10,1}}\big) \\ &\quad - \mathrm{Q}\big(\sqrt{\gamma_{20,1}}\big) - \mathrm{Q}\big(\sqrt{\gamma_{21,1}}\big) - \mathrm{Q}\big(\sqrt{\gamma_{22,1}}\big). \end{aligned} \tag{24}$$

Case 4: The transmitted amplitude is A_{001}. The BER can be computed as the sum of two events, i.e., $P_{B_1}^{(4)} = P_{B_1}^{(4a)} + P_{B_1}^{(4b)}$, where

$$\begin{aligned} P_{B_1}^{(4a)} &= \Pr(w > \{a_{101} + a_{001} - A_{001}\}) \\ &\quad - \Pr(\{a_{011} + a_{101} - A_{001}\} \\ &\qquad < w < \{a_{111} + a_{011} - A_{001}\}) \\ &= \mathrm{Q}\big(\sqrt{\gamma_{8,1}}\big) + \mathrm{Q}\big(\sqrt{\gamma_{11,1}}\big) - \mathrm{Q}\big(\sqrt{\gamma_{23,1}}\big) \end{aligned} \tag{25}$$

and

$$\begin{aligned} P_{B_1}^{(4b)} &= \Pr(w < -A_{001}) \\ &\quad - \Pr(-\{A_{001} + a_{011} + a_{101}\} < w < \\ &\qquad - \{A_{001} + a_{101} + a_{001}\}) \\ &\quad - \Pr(w < -\{A_{001} + a_{111} + a_{011}\}) \\ &= \mathrm{Q}\big(\sqrt{\gamma_{12,1}}\big) + \mathrm{Q}\big(\sqrt{\gamma_{13,1}}\big) \\ &\quad - \mathrm{Q}\big(\sqrt{\gamma_{24,1}}\big) - \mathrm{Q}\big(\sqrt{\gamma_{25,1}}\big). \end{aligned} \tag{26}$$

Thus

$$\begin{aligned} P_{B_1}^{(4)} &= \mathrm{Q}\big(\sqrt{\gamma_{8,1}}\big) + \mathrm{Q}\big(\sqrt{\gamma_{11,1}}\big) + \mathrm{Q}\big(\sqrt{\gamma_{12,1}}\big) + \mathrm{Q}\big(\sqrt{\gamma_{13,1}}\big) \\ &\quad - \mathrm{Q}\big(\sqrt{\gamma_{23,1}}\big) - \mathrm{Q}\big(\sqrt{\gamma_{24,1}}\big) - \mathrm{Q}\big(\sqrt{\gamma_{25,1}}\big). \end{aligned} \tag{27}$$

The cases from 5 to 8 are dropped for brevity. Note that the analysis is identical for both sides. Therefore, the conditional BER can be expressed by

$$P_{B_1|\boldsymbol{\gamma}_1} = \sum_{i=1}^{25} c_i \mathrm{Q}\big(\sqrt{\gamma_{i,1}}\big) \tag{28}$$

where $\mathbf{c} = (1/4)[2, 1, 1, 1, 2, 1, 1, 2, 1, 1, 1, 1, 1, -1, \ldots, -1]$.

B. Middle User (U_2)

Case 1: The BER of this case is

$$\begin{aligned} P_{B_2}^{(1)} &= \Pr(w < -\{A_{111} - a_{011} - a_{101}\}) \\ &\quad - \Pr(-\{A_{111} + a_{011} + a_{101}\} < w < -A_{111}) \\ &= \mathrm{Q}\big(\sqrt{\gamma_{1,2}}\big) + \mathrm{Q}\big(\sqrt{\gamma_{2,2}}\big) - \mathrm{Q}\big(\sqrt{\gamma_{8,2}}\big). \end{aligned} \tag{29}$$

Case 2: The BER of this case is

$$\begin{aligned} P_{B_2}^{(2)} &= \Pr(w < -\{A_{011} - a_{011} - a_{101}\}) \\ &\quad - \Pr(-\{A_{011} + a_{011} + a_{101}\} < w < -A_{011}) \\ &= \mathrm{Q}\big(\sqrt{\gamma_{3,2}}\big) + \mathrm{Q}\big(\sqrt{\gamma_{4,2}}\big) - \mathrm{Q}\big(\sqrt{\gamma_{9,2}}\big). \end{aligned} \tag{30}$$

Case 3: The BER can be computed as the sum of two events, i.e., $P_{B_2}^{(3)} = P_{B_2}^{(3a)} + P_{B_2}^{(3b)}$, where in (33)

$$\begin{aligned} P_{B_2}^{(3a)} &= \Pr(w > \{a_{011} + a_{101} - A_{101}\}) \\ &= \mathrm{Q}\big(\sqrt{\gamma_{3,2}}\big) \end{aligned} \tag{31}$$

and

$$\begin{aligned} P_{B_2}^{(3b)} &= \Pr(w < -A_{101}) \\ &\quad - \Pr(w < -\{A_{101} + a_{011} + a_{101}\}) \\ &= \mathrm{Q}\big(\sqrt{\gamma_{5,2}}\big) - \mathrm{Q}\big(\sqrt{\gamma_{10,2}}\big). \end{aligned} \tag{32}$$

Thus

$$P_{B_2}^{(3)} = \mathrm{Q}\big(\sqrt{\gamma_{3,2}}\big) + \mathrm{Q}\big(\sqrt{\gamma_{5,2}}\big) - \mathrm{Q}\big(\sqrt{\gamma_{10,2}}\big). \tag{33}$$

Case 4: Similarly, the BER can be computed as the sum of two events, i.e., $P_{B_2}^{(4)} = P_{B_2}^{(4a)} + P_{B_2}^{(4b)}$, where

$$\begin{aligned} P_{B_2}^{(4a)} &= \Pr(w > \{a_{011} + a_{101} - A_{001}\}) \\ &= \mathrm{Q}\big(\sqrt{\gamma_{6,2}}\big) \end{aligned} \tag{34}$$

and

$$\begin{aligned} P_{B_2}^{(4b)} &= \Pr(w < -A_{001}) \\ &\quad - \Pr(w < -\{A_{001} + a_{011} + a_{101}\}) \\ &= \mathrm{Q}\big(\sqrt{\gamma_{7,2}}\big) - \mathrm{Q}\big(\sqrt{\gamma_{11,2}}\big). \end{aligned} \tag{35}$$

Thus

$$P_{B_2}^{(4)} = \mathrm{Q}\big(\sqrt{\gamma_{6,2}}\big) + \mathrm{Q}\big(\sqrt{\gamma_{7,2}}\big) - \mathrm{Q}\big(\sqrt{\gamma_{11,2}}\big). \tag{36}$$

Finally, the conditional BER can be written as

$$P_{B_2|\boldsymbol{\gamma}_2} = \sum_{i=1}^{11} c_i \mathrm{Q}\big(\sqrt{\gamma_{i,2}}\big) \tag{37}$$

where $\mathbf{c} = (1/4)[1, 1, 2, 1, 1, 1, 1, -1, \ldots, -1]$.

C. Far User (U_3)

Similarly, the bit error probability for Cases 1–4 are given in (38)–(41), respectively

$$\begin{aligned} P_{B_3}^{(1)} &= \Pr(w < -A_{111}) \\ &= \mathrm{Q}\big(\sqrt{\gamma_{1,3}}\big) \end{aligned} \tag{38}$$

$$\begin{aligned} P_{B_3}^{(2)} &= \Pr(w < -A_{011}) \\ &= \mathrm{Q}\big(\sqrt{\gamma_{2,3}}\big) \end{aligned} \tag{39}$$

$$\begin{aligned} P_{B_3}^{(3)} &= \Pr(w < -A_{101}) \\ &= \mathrm{Q}\big(\sqrt{\gamma_{3,3}}\big) \end{aligned} \tag{40}$$

$$\begin{aligned} P_{B_3}^{(4)} &= \Pr(w < -A_{001}) \\ &= \mathrm{Q}\big(\sqrt{\gamma_{4,3}}\big). \end{aligned} \tag{41}$$

Thus, the conditional BER for the far user is

$$P_{B_3|\boldsymbol{\gamma}_3} = \sum_{i=1}^{4} c_i \mathrm{Q}\big(\sqrt{\gamma_{i,3}}\big) \tag{42}$$

where $\mathbf{c} = (1/4)[1, 1, 1, 1]$.

V. Unconditional BER Analysis

The conditioning can be eliminated by averaging the conditional BER over the PDF of $\boldsymbol{\gamma}_n$

$$P_{B_n} = \int_0^\infty P_{B_n|\boldsymbol{\gamma}_n}\, p\big(\boldsymbol{\gamma}_n\big) d\boldsymbol{\gamma}_n. \tag{43}$$

By substituting the general representation of P_{B_n} in (43), we obtain

$$P_{B_n} = \sum_{i=1}^{L} c_i \int_0^\infty \mathrm{Q}\big(\sqrt{\gamma_{i,n}}\big) p\big(\gamma_{i,n}\big) d\gamma_{i,n} \tag{44}$$

where $\gamma_{i,n} = |h_n|^2 \beta_n G_{i,n}/\sigma_{w_n}^2$ and $G_{i,n}$ is a constant. By noting that h_n is a complex Gaussian random variable, then $|h_n|$ is Rayleigh distributed, and $\eta_n \triangleq |h_n|^2$ is exponentially distributed. Therefore, the PDF of $\gamma_{i,n}$ is exponential as well

$$p\big(\gamma_{i,n}\big) = \frac{1}{\overline{\gamma}_{i,n}} \exp\left(\frac{-\gamma_{i,n}}{\overline{\gamma}_{i,n}}\right). \tag{45}$$

Using the Craig representation of the Q-function

$$\mathrm{Q}(x) = \frac{1}{\pi} \int_0^{\pi/2} \exp\left(\frac{-x^2}{2\sin^2\theta}\right) d\theta \tag{46}$$

and the generation function (MGF) of the exponential PDF [32], the BER expression can be written as

$$\begin{aligned} P_{B_n} &= \sum_{i=1}^{L} \frac{1}{\pi} c_i \int_0^{\pi/2} M_{\gamma_{i,n}}\left(\frac{-\gamma_{i,n}}{2\sin^2\theta}\right) d\theta \\ &= \frac{1}{2} \sum_{i=1}^{L} c_i\, \zeta\big(\gamma_{i,n}\big) \end{aligned} \tag{47}$$

where $M_{\gamma_{i,n}}(-s) = 1/(1 + s\overline{\gamma}_{i,n})$ and c_i is the coefficient multiplied by the Gaussian function in the conditional BER. Also, $\zeta(\gamma_{i,n}) = 1 - \sqrt{0.5\overline{\gamma}_{i,n}/(1 + 0.5\overline{\gamma}_{i,n})}$.

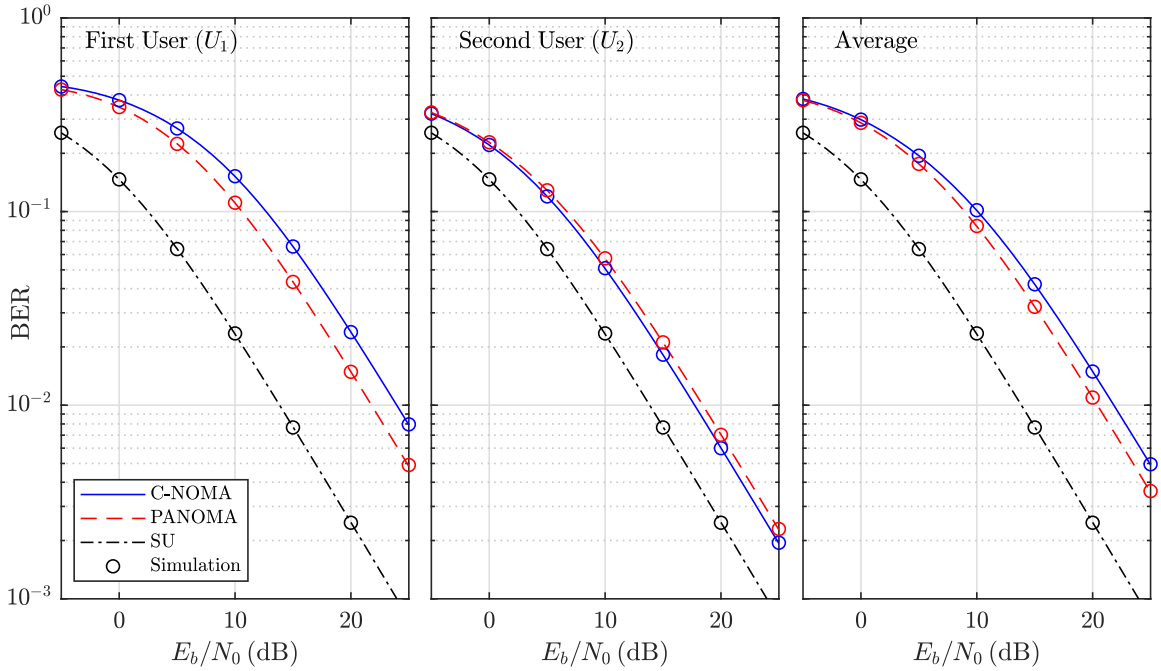

Fig. 4. Analytical and simulated BER results of C-NOMA and PANOMA using BPSK, where $N = 2$.

VI. Channel Capacity

The channel capacity for the nth user is defined as maximum achievable mutual information $I(X_n, Y_n)$ between the channel input X_n and output Y_n when computed over all possible input probability distributions $p(x_n)$ [33, p. 183]

$$C_n = \max_{p(x_n)} I(X_n; Y_n). \tag{48}$$

The mutual information can be expressed as

$$I(X_n; Y_n) = H(X_n) - H(X_n \mid Y_n) \tag{49}$$

where $H(X_n)$ is the entropy of the source and $H(X_n|Y_n)$ is the conditional entropy. For BPSK modulation, the channel between the data source at the base station and detector output of the nth user can be considered as a binary symmetric channel (BSC). Therefore, (48) is maximized when the source binary data symbols are equally likely, which implies that $H(X_n) = 1$ and

$$\begin{aligned} H(X_n|Y_n) &\triangleq \Omega\big(P_{B_n}\big) \\ &= \acute{P}_{B_n} \log_2\left(\frac{1}{\acute{P}_{B_n}}\right) + P_{B_n} \log_2\left(\frac{1}{P_{B_n}}\right) \end{aligned} \tag{50}$$

where $\acute{P}_{B_n} = 1 - P_{B_n}$. Therefore

$$C_n = 1 - \Omega\big(P_{B_n}\big) \tag{51}$$

and thus, the system capacity is given as $C = \sum_{n=1}^{N} C_n$, which is considered a lower bound to the channel symmetric capacity [34], [35].

VII. Numerical Results and Discussion

This section presents the analytical and simulation results for the BER and capacity of the downlink conventional NOMA and proposed PANOMA systems. For more clarity, the conventional NOMA will be denoted as (C-NOMA). The results are presented for $N = 2$ and $N = 3$ cases, using BPSK and gray-coded QPSK modulation. The performance of an SU OMA with maximum transmit power and located at a distance d_1 from the base station is used as a benchmark. The BER and capacity are computed analytically for BPSK and validated by Monte Carlo simulation, while Monte Carlo simulation is used to evaluate the performance using QPSK. In each simulation run, 3×10^7 independent bits are generated with equal probability. The simulations were conducted using a workstation equipped with 2.5-GHz 64 bits quad-core Intel Core i7

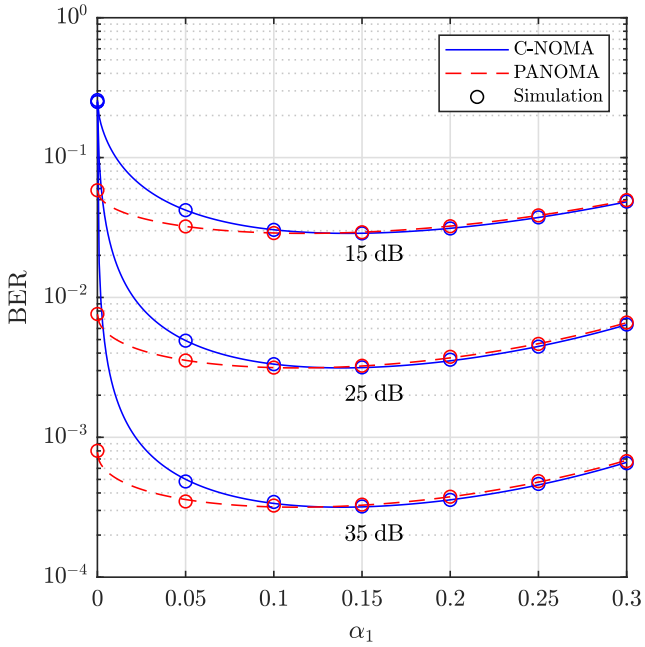

Fig. 5. Analytical and simulated average BER versus α_1 for C-NOMA and PANOMA using BPSK, where $N = 2$.

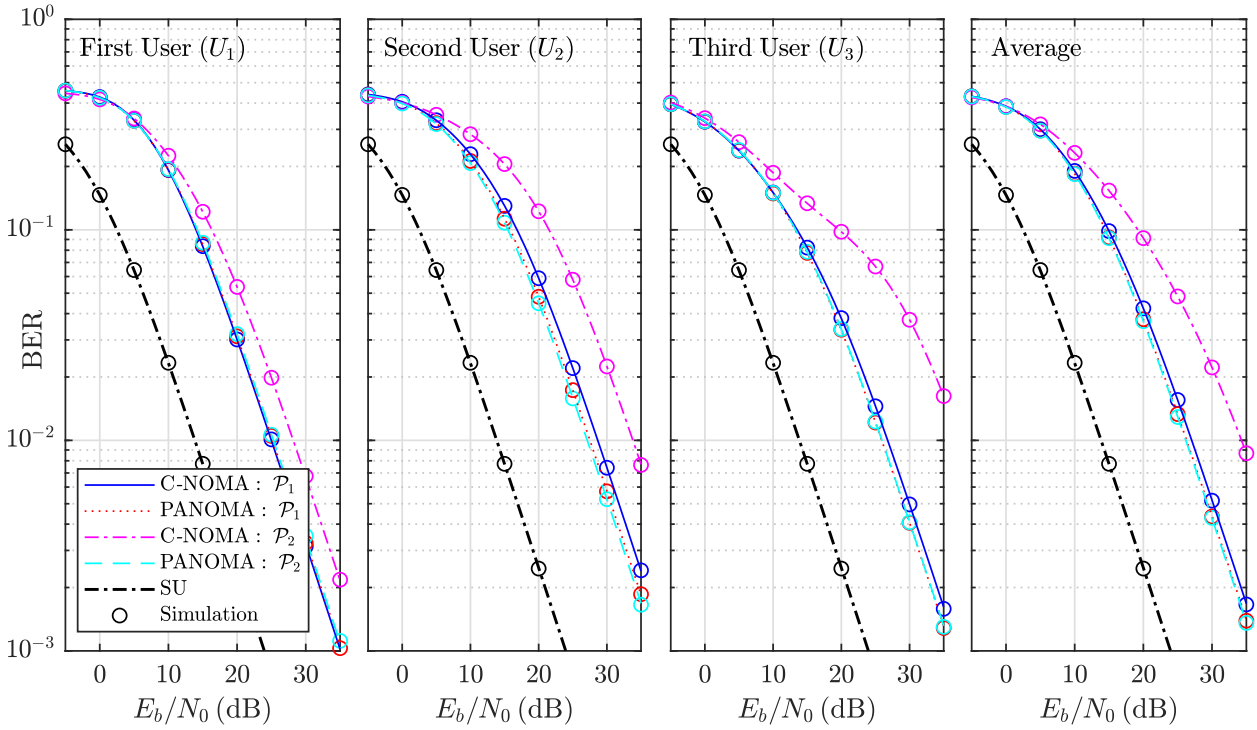

Fig. 6. Analytical and simulated BER results of C-NOMA and PANOMA systems using BPSK for the power assignment of $\mathcal{P}_1$ and $\mathcal{P}_2$, where $N = 3$.

processor and 16-GB RAM. Moreover, the MATLAB Parallel Computing Toolbox was configured to perform parallel computing using four cores. The small-scale fading is considered to be flat and the channel fading coefficients for each realization are modeled as i.i.d. Rayleigh random variables with $\sigma_{h_n}^2 = 1$. The large-scale fading is considered as fixed path loss with an exponent of $\lambda = 2.7$. The users' distances from the base station are, respectively, given by d_1, $d_2 = 1.67d_1$ and $d_3 = 2.78d_1$. Consequently, the path-loss coefficients are $\beta_1 = 0$ dB, $\beta_2 = 6$ dB, and $\beta_3 = 12$ dB. Hence, U_1 can be considered as the near user, while U_2 and U_3 are the middle and far users for $N = 3$. For $N = 2$, U_2 is the far user. The base station and all users are assumed to be equipped with a single antenna. Unless it is mentioned otherwise, all the results for the $N = 2$ case are obtained using fixed power assignment with factors of $\alpha_1 = 0.05$ and $\alpha_2 = 0.95$, where the PANOMA power is assigned as described in (5). For the $N = 3$ case, two fixed power assignment patterns are adopted which are $\mathcal{P}_1 = \{0.05, 0.15, 0.80\}$ and $\mathcal{P}_2 = \{0.1, 0.2, 0.7\}$, where the first value in each pattern corresponds to α_1, while the second and third values correspond to α_2 and α_3. It is important to mention that for PANOMA, these power coefficients are used for Cases 3 and 6, while the rest of cases' power values follow those in Table II.

Fig. 4 shows the BER of the C-NOMA and PANOMA systems using BPSK, where $N = 2$. Although the power assignment for both systems is not optimal, it can be noted that PANOMA outperforms C-NOMA by 2.18 dB for U_1, while a degradation of about 0.7 dB is obtained for U_2. However, the average BER of both users, $(P_{B_1} + P_{B_2})/2$, which is typically considered as the key metric [14], [15], [36], improves by about 1.41 dB. Such degradation is justified by the fact that the power assignment process in the PANOMA is designed to minimize the average BER, not the BER of the individual users. It can be noted from Fig. 4 that the analytical and simulation results match very well for considered scenarios. The same observation is also applicable to Figs. 5, 6, and 9.

Fig. 5 shows the average BER versus α_1 at E_b/N_0 of 15, 25, and 35 dB. It can be noted from the figure that PANOMA average BER degrades slightly as compared to C-NOMA when α_1 deviates from the optimal power for both systems. When the value of α_1 is substantially different from the optimal, the average BER of both systems converges. Moreover, it can be noted that C-NOMA BER is highly sensitive for $\alpha_1 < 0.1$, where the degradation becomes severe.

Fig. 6 is presented to demonstrate the effect of power allocation on the BER of the C-NOMA and PANOMA systems for $N = 3$ case. Therefore, two different power assignments are used which are $\mathcal{P}_1$ and $\mathcal{P}_2$. It is worthy to mention that $\mathcal{P}_1$ is considered optimal for the C-NOMA system at high SNR values. As can be noted from the figure, for $\mathcal{P}_1$, both systems offer approximately the same BER even though the PANOMA power assignment is not optimal. For $\mathcal{P}_2$, which is near optimal for PANOMA and nonoptimal for the C-NOMA, the PANOMA BER remained almost unchanged, while the C-NOMA suffered a drastic degradation, which confirms that PANOMA is robust against the imperfect power allocation that might be caused by imperfect CSI at the transmitter. More specifically, the PANOMA has an advantage of 8.1 dB in the average BER as compared to C-NOMA when both systems use $\mathcal{P}_2$. Furthermore, when comparing the average BER performance of $N = 3$ with $N = 2$, it is noted that the average BER performance is degraded for $N = 3$ because of the increased IUI.

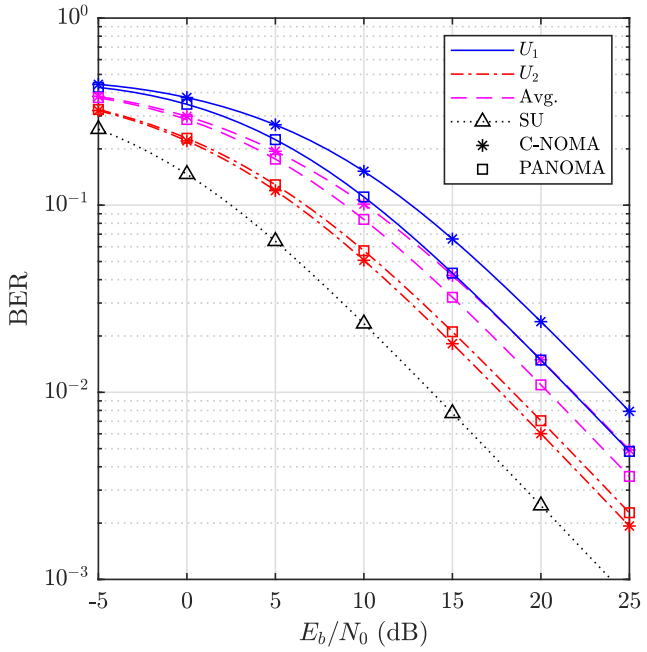

Fig. 7. Simulated BER results of C-NOMA and PANOMA systems using QPSK, where $N = 2$.

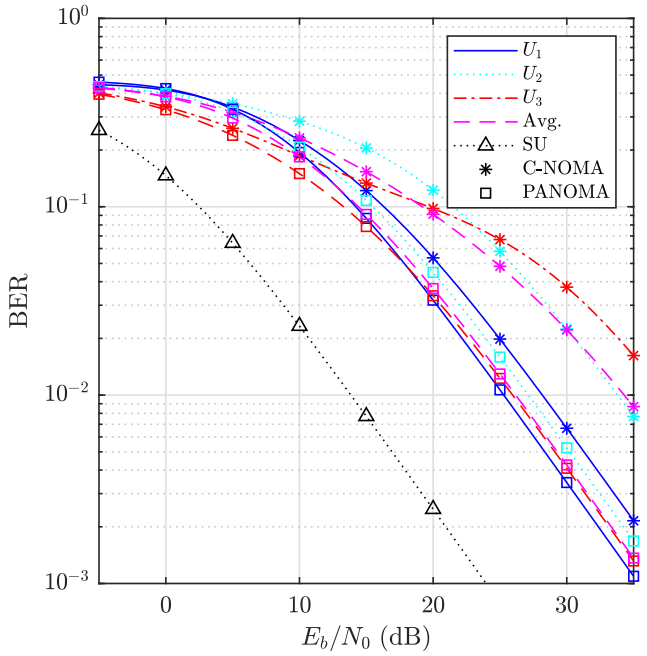

Fig. 8. Simulated BER results of C-NOMA and PANOMA systems using QPSK, where the power assignment follows $\mathcal{P}_2$ and $N = 3$.

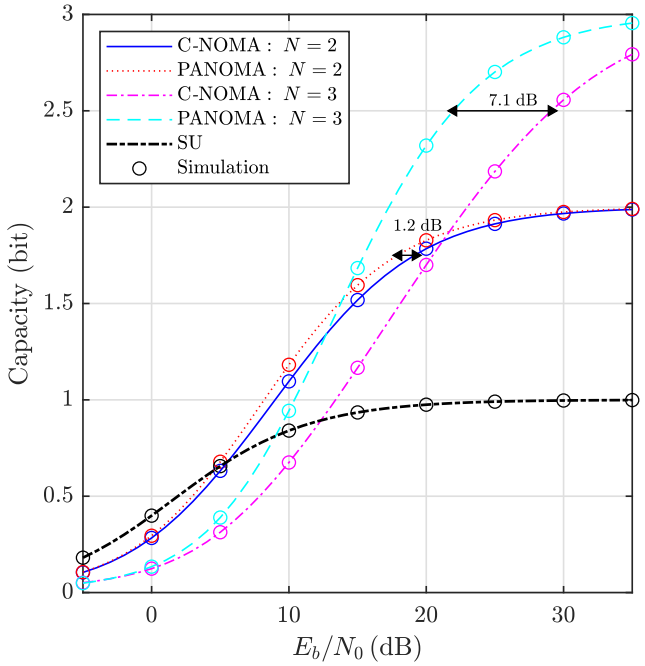

Fig. 9. Analytical and simulated capacity for C-NOMA and PANOMA systems using BPSK, where the power assignment follows $\mathcal{P}_2$ and $N = 3$.

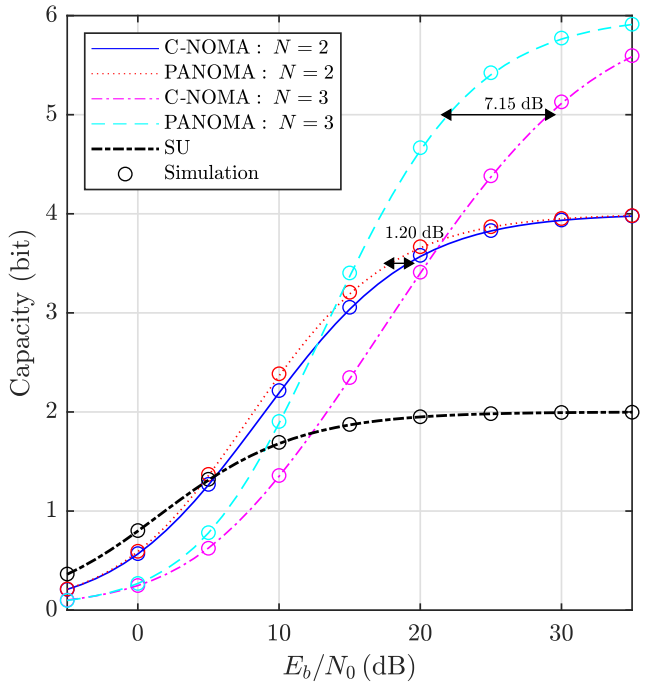

Fig. 10. Analytical and simulated capacity for C-NOMA and PANOMA using QPSK, where the power assignment follows $\mathcal{P}_2$ and $N = 3$.

Figs. 7 and 8 show the BER results of C-NOMA and PANOMA systems using QPSK for $N = 2$ and $N = 3$. As can be noted from both figures, the BER for QPSK is identical to BPSK, which confirms the efficiency of the PANOMA. Moreover, the obtained results follow the SU modulations in which BPSK and QPSK have similar BERs. Nevertheless, BPSK is more robust to CSI estimation errors [37].

Figs. 9 and 10 quantify the PANOMA gain with respect to the achieved system capacity for $N = 2$ and $N = 3$ cases considering BPSK and QPSK, where the power allocation is similar to that in Figs. 7 and 8. For example, when $N = 2$, the maximum gain is 1.2 dB for BPSK and QPSK. In addition, for $N = 3$, the maximum gain is about 7.1 and 7.15 dB for BPSK and QPSK, respectively. As can be noted from both figures, the capacity of PANOMA and C-NOMA decreases and approaches zero when the SNR is decreased. Such behavior is obtained because the capacity at low SNR is dominated by the AWGN, and thus, reducing the IUI or optimizing the power will have a very limited impact on the system performance.

TABLE III
DEFINITIONS OF $\gamma_{l,n}$, $N = 2$

$\gamma_{1,1}$	$\frac{(A_{11}-A_{01})^2}{4\omega_1^{-1}}$	$\gamma_{5,1}$	$\frac{(A_{11}+3A_{01})^2}{4\omega_1^{-1}}$
$\gamma_{2,1}$	$\frac{(3A_{11}+A_{01})^2}{4\omega_1^{-1}}$	$\gamma_{1,2}$	$\frac{(A_{11})^2}{\omega_2^{-1}}$
$\gamma_{3,1}$	$\frac{(A_{01})^2}{\omega_1^{-1}}$	$\gamma_{2,2}$	$\frac{(A_{01})^2}{\omega_2^{-1}}$
$\gamma_{4,1}$	$\frac{(A_{11})^2}{\omega_1^{-1}}$		

TABLE IV
DEFINITIONS OF $\gamma_{l,n}$, $N = 3$

$\gamma_{1,1}$	$\frac{(A_{111}-A_{011})^2}{4\omega_1^{-1}}$	$\gamma_{21,1}$	$\frac{(A_{101})^2}{\omega_1^{-1}}$
$\gamma_{2,1}$	$\frac{(2A_{111}-A_{101}-A_{001})^2}{4\omega_1^{-1}}$	$\gamma_{22,1}$	$\frac{(3A_{101}+A_{011})^2}{4\omega_1^{-1}}$
$\gamma_{3,1}$	$\frac{(2A_{111}+A_{101}+A_{001})^2}{4\omega_1^{-1}}$	$\gamma_{23,1}$	$\frac{(A_{011}+A_{101}-2A_{001})^2}{4\omega_1^{-1}}$
$\gamma_{4,1}$	$\frac{(3A_{111}+A_{011})^2}{4\omega_1^{-1}}$	$\gamma_{24,1}$	$\frac{(3A_{001}+A_{101})^2}{4\omega_1^{-1}}$
$\gamma_{5,1}$	$\frac{(A_{011}-A_{101})^2}{4\omega_1^{-1}}$	$\gamma_{25,1}$	$\frac{(2A_{001}+A_{111}+A_{011})^2}{4\omega_1^{-1}}$
$\gamma_{6,1}$	$\frac{(A_{011})^2}{\omega_1^{-1}}$	$\gamma_{1,2}$	$\frac{(2A_{111}-A_{011}-A_{101})^2}{4\omega_2^{-1}}$
$\gamma_{7,1}$	$\frac{(3A_{011}+A_{101})^2}{4\omega_1^{-1}}$	$\gamma_{2,2}$	$\frac{(2A_{111}+A_{011}+A_{101})^2}{4\omega_2^{-1}}$
$\gamma_{8,1}$	$\frac{(A_{101}-A_{001})^2}{4\omega_1^{-1}}$	$\gamma_{3,2}$	$\frac{(A_{011}-A_{101})^2}{4\omega_2^{-1}}$
$\gamma_{9,1}$	$\frac{(3A_{101}+A_{001})^2}{4\omega_1^{-1}}$	$\gamma_{4,2}$	$\frac{(3A_{011}+A_{101})^2}{4\omega_2^{-1}}$
$\gamma_{10,1}$	$\frac{(2A_{101}+A_{111}+A_{011})^2}{4\omega_1^{-1}}$	$\gamma_{5,2}$	$\frac{(A_{101})^2}{\omega_2^{-1}}$
$\gamma_{11,1}$	$\frac{(A_{111}+A_{011}-2A_{001})^2}{4\omega_1^{-1}}$	$\gamma_{6,2}$	$\frac{(A_{011}+A_{101}-2A_{001})^2}{4\omega_2^{-1}}$
$\gamma_{12,1}$	$\frac{(A_{001})^2}{\omega_1^{-1}}$	$\gamma_{7,2}$	$\frac{(A_{001})^2}{\omega_2^{-1}}$
$\gamma_{13,1}$	$\frac{(2A_{001}+A_{011}+A_{101})^2}{4\omega_1^{-1}}$	$\gamma_{8,2}$	$\frac{(A_{111})^2}{\omega_2^{-1}}$
$\gamma_{14,1}$	$\frac{(2A_{111}-A_{011}-A_{101})^2}{4\omega_1^{-1}}$	$\gamma_{9,2}$	$\frac{(A_{011})^2}{\omega_2^{-1}}$
$\gamma_{15,1}$	$\frac{(A_{111})^2}{\omega_1^{-1}}$	$\gamma_{10,2}$	$\frac{(3A_{101}+A_{011})^2}{4\omega_2^{-1}}$
$\gamma_{16,1}$	$\frac{(2A_{111}+A_{011}+A_{101})^2}{4\omega_1^{-1}}$	$\gamma_{11,2}$	$\frac{(2A_{001}+A_{011}+A_{101})^2}{4\omega_2^{-1}}$
$\gamma_{17,1}$	$\frac{(2A_{011}-A_{101}-A_{001})^2}{4\omega_1^{-1}}$	$\gamma_{1,3}$	$\frac{(A_{111})^2}{\omega_3^{-1}}$
$\gamma_{18,1}$	$\frac{(2A_{011}+A_{101}+A_{001})^2}{4\omega_1^{-1}}$	$\gamma_{2,3}$	$\frac{(A_{011})^2}{\omega_3^{-1}}$
$\gamma_{19,1}$	$\frac{(3A_{011}+A_{111})^2}{4\omega_1^{-1}}$	$\gamma_{3,3}$	$\frac{(A_{101})^2}{\omega_3^{-1}}$
$\gamma_{20,1}$	$\frac{(A_{111}+A_{011}-2A_{101})^2}{4\omega_1^{-1}}$	$\gamma_{4,3}$	$\frac{(A_{001})^2}{\omega_3^{-1}}$

By increasing the SNR, the impact of the proposed power assignment becomes more apparent.

VIII. CONCLUSION AND FUTURE WORK

This article proposed an efficient power assignment scheme to improve the BER performance of NOMA-IoT systems by increasing the system tolerance to nonoptimal power assignment. Exact closed-form analytical BER and lower bound capacity expressions were derived for the JMLD receiver of both C-NOMA and PANOMA over Rayleigh fading channels, where the cases of two and three users were considered. These expressions were verified via Monte Carol simulation results, which showed that the proposed PANOMA is superior in terms of BER and capacity. This demonstrated the ability of PANOMA to operate effectively under nonoptimal power allocation, which is typically caused by the lack of accurate CSI at the transmitter. Moreover, it can be noted that the performance gain achieved using PANOMA is maintained even when the number of users increased from two to three. The same conclusion can be also made for the capacity results where the PANOMA outperformed the NOMA. Furthermore, when PANOMA was applied to QPSK, the performance improvement was identical to the BPSK case.

As the analytical BER and capacity analysis in this work focus on the two and three users scenarios, our future work will aim at generalizing the BER and capacity analysis to include the large number of users and higher order modulations schemes.

APPENDIX
DEFINITIONS OF $\gamma_{l,n}$

The definitions of $\gamma_{l,n}$ are listed in Tables III and IV. Note that $\omega_n = [(|H_n|^2)/(\sigma_w^2)]$.

REFERENCES

[1] M. Shirvanimoghaddam, M. Dohler, and S. J. Johnson, "Massive non-orthogonal multiple access for cellular IoT: Potentials and limitations," *IEEE Commun. Mag.*, vol. 55, no. 9, pp. 55–61, Sep. 2017.

[2] A. J. Al-Dweik, M. Mayhew, R. Muresan, S. M. Ali, and A. Shami, "Using technology to make roads safer: Adaptive speed limits for an intelligent transportation system," *IEEE Veh. Technol. Mag.*, vol. 12, no. 1, pp. 39–47, Mar. 2017.

[3] A. Al-Dweik, R. Muresan, M. Mayhew, and M. Lieberman, "IoT-based multifunctional scalable real-time enhanced road side unit for intelligent transportation systems," in *Proc. IEEE 30th Can. Conf. Elect. Comput. Eng. (CCECE)*, Windsor, ON, Canada, Mar. 2017, pp. 1–6.

[4] L. Yang, R. Muresan, A. Al-Dweik, and L. J. Hadjileontiadis, "Image-based visibility estimation algorithm for intelligent transportation systems," *IEEE Access*, vol. 6, pp. 76728–76740, 2018.

[5] Y. Liu, Z. Qin, M. Elkashlan, Z. Ding, A. Nallanathan, and L. Hanzo, "Nonorthogonal multiple access for 5G and beyond," *Proc. IEEE*, vol. 105, no. 12, pp. 2347–2381, Dec. 2017.

[6] L. Dai, B. Wang, Z. Ding, Z. Wang, S. Chen, and L. Hanzo, "A survey of non-orthogonal multiple access for 5G," *IEEE Commun. Surveys Tuts.*, vol. 20, no. 3, pp. 2294–2323, 3rd Quart., 2018.

[7] A. Hoglund *et al.*, "Overview of 3GPP release 14 enhanced NB-IoT," *IEEE Netw.*, vol. 31, no. 6, pp. 16–22, Nov./Dec. 2017.

[8] M. A. Al-Jarrah, M. A. Yaseen, A. Al-Dweik, O. A. Dobre, and E. Alsusa, "Decision fusion for IoT-based wireless sensor networks," *IEEE Internet Things J.*, vol. 7, no. 2, pp. 1313–1326, Feb. 2020.

[9] Y. Saito, Y. Kishiyama, A. Benjebbour, T. Nakamura, A. Li, and K. Higuchi, "Non-orthogonal multiple access (NOMA) for cellular future radio access," in *Proc. IEEE 77th Veh. Technol. Conf. (VTC)*, Dresden, Germany, Jun. 2013, pp. 1–5.

[10] N. I. Miridakis and D. D. Vergados, "A survey on the successive interference cancellation performance for single-antenna and multiple-antenna OFDM systems," *IEEE Commun. Surveys Tuts.*, vol. 15, no. 1, pp. 312–335, 1st Quart., 2013.

[11] R. Zhang and L. Hanzo, "A unified treatment of superposition coding aided communications: Theory and practice," *IEEE Commun. Surveys Tuts.*, vol. 13, no. 3, pp. 503–520, 3rd Quart., 2011.

[12] H. Marshoud, P. C. Sofotasios, S. Muhaidat, G. K. Karagiannidis, and B. S. Sharif, "On the performance of visible light communication systems with non-orthogonal multiple access," *IEEE Trans. Wireless Commun.*, vol. 16, no. 10, pp. 6350–6364, Oct. 2017.

[13] F. Kara and H. Kaya, "BER performances of downlink and uplink NOMA in the presence of SIC errors over fading channels," *IET Commun.*, vol. 12, no. 15, pp. 1834–1844, Sep. 2018.

[14] L. Bariah, S. Muhaidat, and A. Al-Dweik, "Error probability analysis of non-orthogonal multiple access over Nakagami-*m* fading channels," *IEEE Trans. Commun.*, vol. 67, no. 2, pp. 1586–1599, Feb. 2019.

[15] T. Assaf, A. Al-Dweik, M. E. Moursi, and H. Zeineldin, "Exact BER performance analysis for downlink NOMA systems over Nakagami-*m* fading channels," *IEEE Access*, vol. 7, pp. 134539–134555, 2019.

[16] T. Assaf, A. J. Al-Dweik, M. S. E. Moursi, H. Zeineldin, and M. Al-Jarrah, "Exact bit error-rate analysis of two-user NOMA using QAM with arbitrary modulation orders," *IEEE Commun. Lett.*, vol. 24, no. 12, pp. 2705–2709, Dec. 2020.

[17] E. C. Cejudo, H. Zhu, and O. Alluhaibi, "On the power allocation and constellation selection in downlink NOMA," in *Proc. IEEE 86th Veh. Technol. Conf. (VTC)*, Toronto, ON, Canada, Sep. 2017, pp. 1–5.

[18] M. Aldababsa, C. Göztepe, G. K. Kurt, and O. Kucur, "Bit error rate for NOMA network," *IEEE Commun. Lett.*, vol. 24, no. 6, pp. 1188–1191, Jun. 2020.

[19] H. Yahya, E. Alsusa, and A. Al-Dweik. (Nov. 2020). *Exact BER Analysis of NOMA With Arbitrary Number of Users and Modulation Orders*. [Online]. Available: https://doi.org/10.36227/techrxiv.13229210.v1

[20] B. Selim, S. Muhaidat, P. C. Sofotasios, A. Al-Dweik, B. S. Sharif, and T. Stouraitis, "Radio-frequency front-end impairments: Performance degradation in nonorthogonal multiple access communication systems," *IEEE Veh. Technol. Mag.*, vol. 14, no. 1, pp. 89–97, Mar. 2019.

[21] X. Wan, X. Zhu, Y. Jiang, Y. Liu, and J. Zhao, "An interference alignment and ICA-based semiblind dual-user downlink NOMA system for high-reliability low-latency IoT," *IEEE Internet Things J.*, vol. 7, no. 11, pp. 10837–10851, Nov. 2020.

[22] J. Chu, X. Chen, C. Zhong, and Z. Zhang, "Robust design for NOMA-based multibeam LEO satellite Internet of Things," *IEEE Internet Things J.*, vol. 8, no. 3, pp. 1959–1970, Feb. 2021.

[23] Y. Xu, R. Q. Hu, and G. Li, "Robust energy-efficient maximization for cognitive NOMA networks under channel uncertainties," *IEEE Internet Things J.*, vol. 7, no. 9, pp. 8318–8330, Sep. 2020.

[24] Q. Qi, X. Chen, and D. W. K. Ng, "Robust beamforming for NOMA-based cellular massive IoT with SWIPT," *IEEE Trans. Signal Process.*, vol. 68, pp. 211–224, 2020, doi: 10.1109/TSP.2019.2959246.

[25] J. Zhang, X. Wang, T. Hasegawa, and T. Kubo, "Downlink non-orthogonal multiple access (NOMA) constellation rotation," in *Proc. IEEE 84th Veh. Technol. Conf. (VTC)*, Montreal, QC, Canada, Sep. 2016, pp. 1–5.

[26] M. Qiu, Y.-C. Huang, and J. Yuan, "Downlink non-orthogonal multiple access without SIC for block fading channels: An algebraic rotation approach," *IEEE Trans. Wireless Commun.*, vol. 18, no. 8, pp. 3903–3918, Aug. 2019.

[27] *Technical Specification Group Radio Access Network; Evolved Universal Terrestrial Radio Access (E-UTRA); Physical Channels and Modulation, (Release 10)*, ETSI Standard GPP TS 36.211 V10.5.0, Jun. 2012.

[28] T. Assaf, A. Al-Dweik, M. S. E. Moursi, H. Zeineldin, and M. Al-Jarrah, "NOMA receiver design for delay-sensitive systems," *IEEE Syst. J.*, early access, Nov. 9, 2020, doi: 10.1109/JSYST.2020.3032878.

[29] E. Alsusa and C. Masouros, "Adaptive code allocation for interference management on the downlink of DS-CDMA systems," *IEEE Trans. Wireless Commun.*, vol. 7, no. 7, pp. 2420–2424, Jul. 2008.

[30] C. Masouros and E. Alsusa, "Dynamic linear precoding for the exploitation of known interference in MIMO broadcast systems," *IEEE Trans. Wireless Commun.*, vol. 8, no. 3, pp. 1396–1404, Mar. 2009.

[31] *IEEE Standard for Information Technology—Telecommunications and Information Exchange Between Systems Local and Metropolitan Area Networks—Specific Requirements—Part 11: Wireless LAN Medium Access Control (MAC) and Physical Layer (PHY) Specifications*, IEEE Standard 802.11-2016, 2016.

[32] M. Simon and M. Alouini, *Digital Communication Over Fading Channels*, 2nd ed. Hoboken, NJ, USA: Wiley, 2005.

[33] T. M. Cover and J. A. Thomas, *Elements of Information Theory*, 2nd ed. Hoboken, NJ, USA: Wiley, 2006.

[34] T. F. Wong, "Numerical calculation of symmetric capacity of rayleigh fading channel with BPSK/QPSK," *IEEE Commun. Lett.*, vol. 5, no. 8, pp. 328–330, Aug. 2001.

[35] E. Baccarelli and A. Fasano, "Some simple bounds on the symmetric capacity and outage probability for QAM wireless channels with Rice and Nakagami fadings," *IEEE J. Sel. Areas Commun.*, vol. 18, no. 3, pp. 361–368, Mar. 2000.

[36] Q.-Y. Yu, H.-H. Chen, and W.-X. Meng, "A unified multiuser coding framework for multiple-access technologies," *IEEE Syst. J.*, vol. 13, no. 4, pp. 3781–3792, Dec. 2019.

[37] A. Saci, A. Al-Dweik, A. Shami, and Y. Iraqi, "One-shot blind channel estimation for OFDM systems over frequency-selective fading channels," *IEEE Trans. Commun.*, vol. 65, no. 12, pp. 5445–5458, Dec. 2017.

Hamad Yahya (Graduate Student Member, IEEE) was born in Sharjah, UAE, in 1997. He received the B.Sc. degree in electrical engineering/communication from Ajman University, Ajman, UAE, in 2018, where he was the top of the class and the M.Sc. degree (with Distinction) in communications and signal processing from The University of Manchester, Manchester, U.K., in 2019, where he is currently pursuing the Ph.D. degree in electrical and electronic engineering.

He is also a Graduate Teaching Assistant with The University of Manchester. His research interests include wireless communications for future wireless networks, optimization, and visible light communication.

Mr. Yahya received the Best Student and the Best Project Prizes from the Department of Electrical and Electronic Engineering, The University of Manchester. He was nominated for the Distinguished Achievement Award in 2019, where he was among the top 14 postgraduate taught students across the Faculty of Science and Engineering. He is the recipient of the M.Sc. Success Scholarship from The University of Manchester.

Arafat Al-Dweik (Senior Member, IEEE) received the M.S. (*summa cum laude*) and Ph.D. (*magna cum laude*) degrees in electrical engineering from Cleveland State University, Cleveland, OH, USA, in 1998 and 2001, respectively.

He is currently with the Department of Electrical Engineering and Computer Science, Khalifa University, Abu Dhabi, UAE. He also worked with Efficient Channel Coding, Inc., Cleveland; the Department of Information Technology, Arab American University, Jenin, Palestine; and the University of Guelph, Guelph, ON, Canada. He is a Visiting Research Fellow with the School of Electrical, Electronic, and Computer Engineering, Newcastle University, Newcastle upon Tyne, U.K., and a Research Professor with Western University, London, ON, Canada, and the University of Guelph. He has extensive research experience in various areas of wireless communications that include modulation techniques, channel modeling and characterization, synchronization and channel estimation techniques, OFDM technology, error detection and correction techniques, MIMO, and resource allocation for wireless networks.

Dr. Al-Dweik was awarded the Fulbright Scholarship from 1997 to 1999. He was the recipient of the Hijjawi Award for Applied Sciences in 2003, the Fulbright Alumni Development Grant in 2003 and 2005, the Dubai Award for Sustainable Transportation in 2016, and the UAE Leader-Founder Award in 2019. He serves as an Associate Editor for the IEEE TRANSACTIONS ON VEHICULAR TECHNOLOGY and the *IET Communications*. He is a Registered Professional Engineer in the Province of Ontario, Canada. He is a member of Tau Beta Pi and Eta Kappa Nu.

Emad Alsusa (Senior Member, IEEE) received the Ph.D. degree in telecommunications from the University of Bath, Bath, U.K., in 2000.

In 2000, he was appointed to work on developing high data rates systems as part of an industrial project based at Edinburgh University, Edinburgh, U.K. He joined Manchester University (then UMIST), Manchester, U.K., in September 2003, as a Faculty Member, where his current rank is a Reader with the Communication Engineering Group. His research interests lie in the area of communication systems with a focus on physical, MAC, and network layers, including developing techniques and algorithms for array signal detection, channel estimation and equalization, adaptive signal precoding, interference avoidance through novel radio resource management techniques, cognitive radio, and energy and spectrum optimization techniques. Applications of his research include cellular networks, IoT, Industry 4.0, and power line communications. His research work has resulted in over 200 journals and refereed conference publications mainly in top IEEE transactions and conferences. He has supervised over 30 Ph.D.s to successful completion.

Dr. Alsusa has received a number of awards, including the Best Paper Award in the International Symposium on Power Line Communications 2016 and the Wireless Communications and Networks Conference 2019. He is an Editor of the IEEE WIRELESS COMMUNICATION LETTERS, a Fellow of the U.K. Higher Academy of Education, and a TPC Track Chair of a number of conferences, such as VTC'16, GISN'16, PIMRC'17, and Globecom'18, as well as the General Co-Chair of the OnlineGreenCom'16 Conference. He is currently the U.K. representative in the International Union of Radio Science, and a Co-Chair of the IEEE Special Working Group on RF Energy Harvesting.